

Original Article

Optimization of Effective Parameters on Acoustic Radiation Force Shear Waves Interference Patterns Elastography by Using a Finite Element Model

Vahid Sadeghi ^{1,2}, Pezhman Pasyar ^{1,2}, Hassan Rezazadeh ^{1,2}, Hossein Arabalibeik ^{3,*}, Bahador Makkiabadi ³, Seyyed Moayyed Alavian ⁴

¹ Department of Medical Physics and Biomedical Engineering, School of Medicine, Tehran University of Medical Sciences, Tehran, Iran

² Research Center for Science and Technology in Medicine, Tehran University of Medical Sciences, Tehran, Iran

³ Research Center of Biomedical Technology and Robotics, Tehran University of Medical Sciences, Tehran, Iran

⁴ Center for Gastroenterology and Liver Disease, Baqiyatallah University of Medical Sciences, Tehran, Iran

Received: 10 April 2018

Accepted: 05 June 2018

Keywords:

Elastography;

Shear Wave;

Elasticity;

Acoustic Radiation Force;

Ultrasound;

Finite Element Model.

ABSTRACT

Purpose: Variations in the mechanical properties of soft tissues may be a sign of a disease. Since some disease like fibrosis or cancer change the stiffness of related tissues, we can assess the disease of a soft tissue with its elasticity. The elastic stiffness properties of soft tissues can be estimated using locally induced displacements and shear waves.

Materials and Methods: A two-dimensional plane finite element model has been created as soft tissue. The soft tissue has been exposed to two Amplitude Modulated High Intensity Focused Ultrasound transducer (AMHIFU), hence shear wave interference patterns which can be captured by lower frame rate imaging are generated. The acoustic radiation force created by a self-focusing ultrasound transducer has been determined from an ultrasound pressure field simulation. A Gaussian function was fitted to the resulting Acoustic Radiation Force (ARF) field and implemented in the form of a body force in the finite element model.

Results: The effect of different excitation parameters for their optimization in the elasticity estimation has been investigated.

Conclusion: In the result section, the effect of ARF excitation parameters on shear wave elasticity measurements has been represented. Shear wave interference pattern elastography which does not need high frame rate imaging with optimized parameters can be used as a non-invasive method for measuring the elastic stiffness of soft tissues.

1. Introduction

Changes in biomechanical properties of soft tissues like stiffness may serve as a marker for diseases such as tumor and fibrosis. Tissue hardness is proportional to its elasticity. As the oldest method, manual palpation is used to determine the stiffness of superficial

organs qualitatively. This method is generally subjective and operator-dependent. The biopsy process, although is the gold standard for staging the hepatic fibrosis [1], has many drawbacks such as error in sampling [2] as well as highly expensive and painful (which can lead to bleeding and infection) [3].

***Corresponding Author:**

Hossein Arabalibeik, PhD

Research Center of Biomedical Technology and Robotics, Tehran University of Medical Sciences, Tehran, Iran

Tel: (+98)2166581505 / Fax: (+98)2166581533.

Email: arabalibeik@tums.ac.ir

Elastography or elasticity imaging is a non-invasive imaging technique for assessing the stiffness of soft tissues. The elasticity imaging process consists of three stages:

- 1) Applying mechanical force to deform soft tissue (stress).
- 2) Imaging the tissue response (strain) to this stress.
- 3) Extracting the elasticity information.

Elastography, based on imaging modality can be divided into ultrasound, Magnetic Resonance Elastography (MRE[4-6]) and Optical Coherent Elastography (OCE) [7-9]. OCE has several advantages such as high resolution and noninvasiveness. It can be used to assess the biomechanical properties of tissues in the micro scale in three dimensions because of its inherent resolution[10]. However, optical elastography has a disadvantage of lesser penetration depth compared to other modalities. The penetration depth of optical elastography methods are limited to a few millimeters beneath the skin. In comparison with MRE, the ultrasound elastography has many advantages such as: more accessible and acceptable for patients, simple instrumentation, low cost and safe, but the most important advantage is the possibility of using ARF instead of the need for an external source.

According to the temporal characteristic of the applied force, elastography can be split into two categories : static [11, 12] and dynamic. In static elastography, the tissue is compressed slowly by a constant force (i.e. manual palpation). This method cannot provide quantitative information due to the unknown stress. For dynamic elastography, an internal (acoustic radiation force) or external (mechanical vibration) force which varies along the time like transient[13] or oscillator is applied to extract quantitative information about tissue elasticity. Dynamic methods such as Shear wave Dispersion Ultrasound Vibrometry (SDUV)[14, 15], Harmonic Motion Imaging (HMI) [16-18], Vibro-Acoustography (VA) [19, 20] Shear Wave Elasticity Imaging (SWEI) [11, 21], (ARFI) imaging [22, 23] and Supersonic Shear Imaging (SSI) [24] all make use of ARF to induce a local displacement and shear wave within the tissue.

Based on the nature of applied forces, elastography methods can be divided into two categories: mechanical excitation (which can be categorized to two classes- pulsatile flow that uses internal excitation source[25] and surface mechanical excitation)[26] and Acoustic Radiation Force (ARF) [27]. Excitation from body surface has this disadvantage that underlying tissues attenuate the amplitude of the force to reach the targeted tissue in depth. Acoustic radiation force-based elasticity imaging uses ARF as a virtual finger to deform the tissue locally at any desired depth [28].

Using two adjacent vibration sources, two generated shear waves move in opposite directions and interfere with each other, leading to the appearance of a mixed shear wave field. If sources had the same phase and frequency, the constructive and destructive waves would have been generated and with slight differences in the phase or frequency, the interference patterns move to the lower frequency source and crawling waves would be generated. We can reach the shear wave speed and elasticity of soft tissues regarding the velocity or distance between the stripes in moving and standing interference patterns, respectively. Unlike many ultrasound elastography methods which need ultrafast imaging, for this case, to record the generated standing wave, ultrafast imaging is not needed.

Wu *et al.* in 2004 used two mechanical stimulators in opposite directions of a phantom to induce crawling waves and a transducer perpendicular to these bimorph actuators to track the crawling wave. Although, due to high attenuation of shear waves and the position of stimulation sources, this configuration was not suitable for the elasticity estimation of soft tissues within the body [26].

In 2010, Hah *et al.* took advantage of two single elements focused ultrasound transducer and other single elements for generating and tracking crawling waves, respectively. Although their set up was useful for elasticity imaging and tumor detection within tissue mimicking phantoms, this process was time-consuming [28].

In 2012, Hoyt *et al.* used two ARF sources to induce a standing interference pattern. They applied Green's function to estimate the shear wave displacement which is efficient in assessing homogeneous tissues [29].

This study is organized as follows: First, we will show the general scheme of the simulation and then describe each step engaged in the simulation process in detail. These steps consist of simulating HIFU transducer with different characteristics, acoustic pressure estimation, acoustic radiation intensity and force calculation. We will also apply the calculated acoustic radiation force to the Finite Element Model (FEM), displacement extraction

from FEM, image formation and post processing. Finally, we will compare the estimated elasticity for various transducer characteristics and end with discussion and conclusion.

2. Materials and Methods

The flowchart for the simulation is shown in Figure 1.

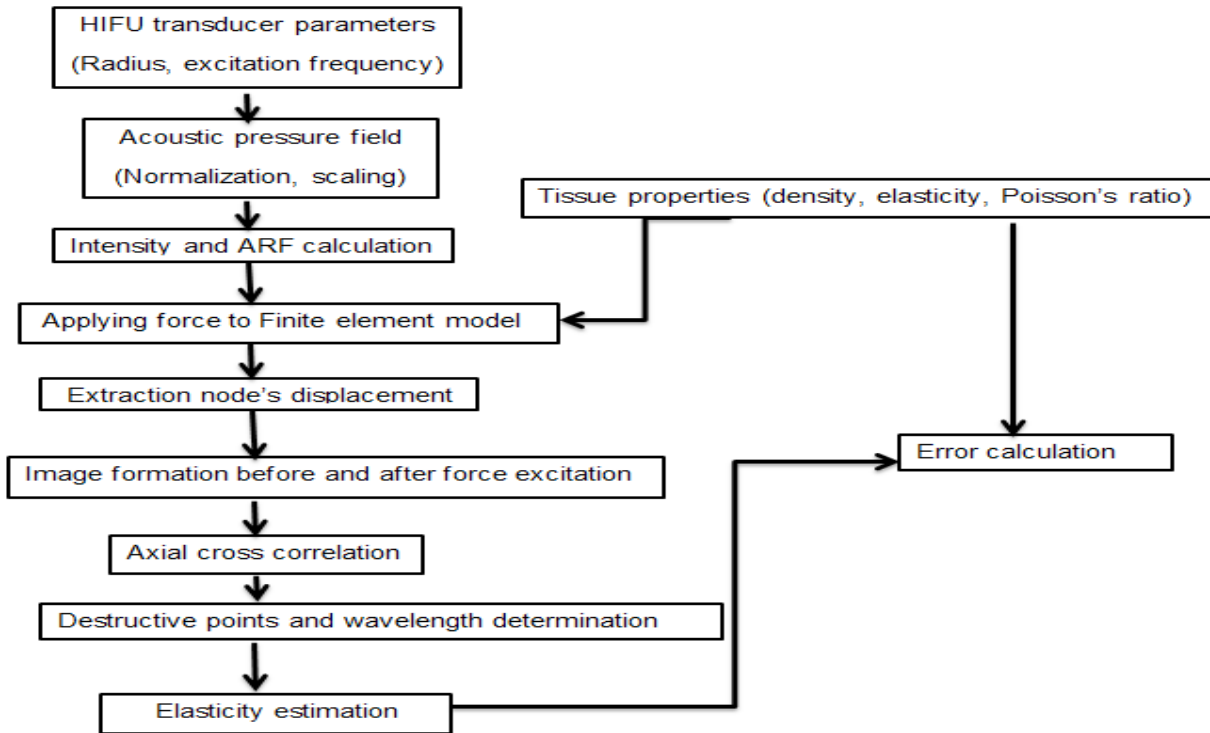


Figure 1. Simulation flowchart

Firstly, we simulated a HIFU transducer with specified parameters in FIELD II and calculated the RMS pressure, intensity and acoustic radiation force in front of HIFU. HIFU transducer has been applied because of its high intensity and focusing nature. The focal spot dimensions of the HIFU are dependent on its excitation frequency and aperture radius. The mentioned parameters are sufficiently large for concentrating the force in the focal point for shear wave creation. Gaussian functions have been fitted to the obtained ARF. For generating shear wave standing interference patterns, this body force from two adjacent points have been applied to the finite element model as the excitation

function while the tissue response was recorded with a low frame rate imaging. With using a finite element software and field II toolbox, ultrasound images have been formed during the shear wave movement, afterwards the scatters' displacement has been obtained by normalizing the cross correlation in the axial direction. Scatters with maximum and minimum displacement are known as nodes and antinodes respectively. The distance between two adjacent nodes is equal to the shear wave wavelength. Elasticity can be computed in terms of modulation frequency and shear wave wavelength. Calculated elasticity was compared to the actual values entered in the FEM model.

Single element transducers which geometrically lead to a focused ultrasound field, utilize a piezoelectric element shaped as a bowl or hollow segment of a sphere and are referred to as spherically focused transducers.

Spherically focused transducers produce acoustic waves which inherently tend to converge to a single focal point and then diverge. The HIFU transducer used in our simulation is a part of a sphere with a 5cm radius which has been cut from different sections with different excitation frequencies. We simulated two Amplitude-Modulated High Intensity Focused Ultrasound (AMHIFU) transducer for inducing the shear wave standing interference pattern. Typical values for HIFU characteristics are listed in Table 1.

Table 1. Typical values for HIFU parameters used in the FIELD II simulation

Parameter	Value	Unit
HIFU aperture radius	15	mm
Focal depth	50	mm
Excitation frequency	1	MHz

We intend to compute the acoustic pressure from HIFU in a linear, isotropic and homogeneous cubic (15*15*15) structure. Due to the symmetry of HIFU transducer and medium, we obtained the acoustic pressure in x-z plane in front of HIFU transducer to reduce the computational load and

time. The FIELD II, a MATLAB-based toolbox was used for modeling the HIFU transducer with various face radius, excitation frequency and calculating the resultant pressure field in the two-dimensional plane with the same axial (z-direction) and lateral (x-direction) dimensions equal to 15cm as well as a pitch size of 1 mm in any direction. Since the values of calculated RMS acoustic pressure in the FIELD II are not real and the minimum RMS acoustic pressure for displacing the tissue in the range of a micrometer is 2.5 MPa, we normalized and scaled the calculated RMS pressure by a typical value of 2.5 MPa. The RMS pressure field of a HIFU with 1 MHz excitation frequency, 20 mm aperture radius and 50 mm focal length is shown in Figure 2.

The acoustic intensity of the HIFU beam with AM wave as input excitation is half of a non-modulated acoustic wave.

$$I = \frac{P_{rms}^2}{4Z}$$

Where $I(\frac{W}{m^2})$, $P_{rms}(pa)$ and $Z(\frac{Kg}{m^2s})$ are temporal average intensity, root mean square pressure and characteristic impedance, respectively.

The characteristic impedance, in turn, can be expressed as follow:

$$Z = \rho C_c$$

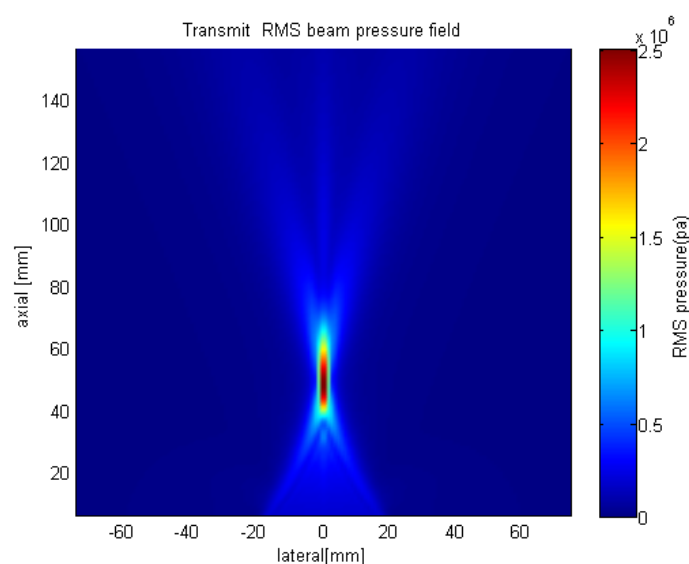


Figure 2. The RMS pressure of a HIFU with 1 MHz excitation frequency, face radius and focal length equal to 20 and 50 mm, respectively

Where $\rho (\frac{Kg}{m^3})$ is the density of tissue and $C_c(\frac{m}{sec})$ is the compressional (longitudinal) wave speed.

When ultrasound waves propagate through tissue, because of absorption and attenuation, energy is absorbed by the tissue and momentum is transferred from wave to tissue, resulting in the generation of acoustic radiation force in the direction of wave propagation. Since the component of ARF in the elevation (y) and lateral (x) directions cancel out each other, we have applied this force in the axial (z) direction. For HIFU transducer, the geometric focal point lies at the center of the imaginary sphere. The piezoelectric element, which is a part of it and the ARF is localized in the focal spot.

The magnitude of this body force is calculated using the equation below [30]:

$$|\vec{F}| = \frac{2\alpha I}{c_c}$$

Where $F(\frac{N}{m^3})$ is the acoustic radiation force, $\alpha(\frac{dB}{cm.MHz})$ is the attenuation coefficient, $I(\frac{W}{m^2})$ is the acoustic intensity and $C_c(\frac{m}{sec})$ is the compressional wave speed. Values for absorption coefficient, density, and longitudinal wave speed were selected in accordance with the soft tissue (i.e. liver) as expressed in Table 2.

Table 2. Typical values of the soft tissue's parameters for ARF calculation

Parameter	Value	Unit
Absorption coefficient	0.7	$\frac{dB}{cm.MHz}$
Density	1000	$\frac{Kg}{m^3}$
Compressional wave speed	1540	$\frac{m}{sec}$

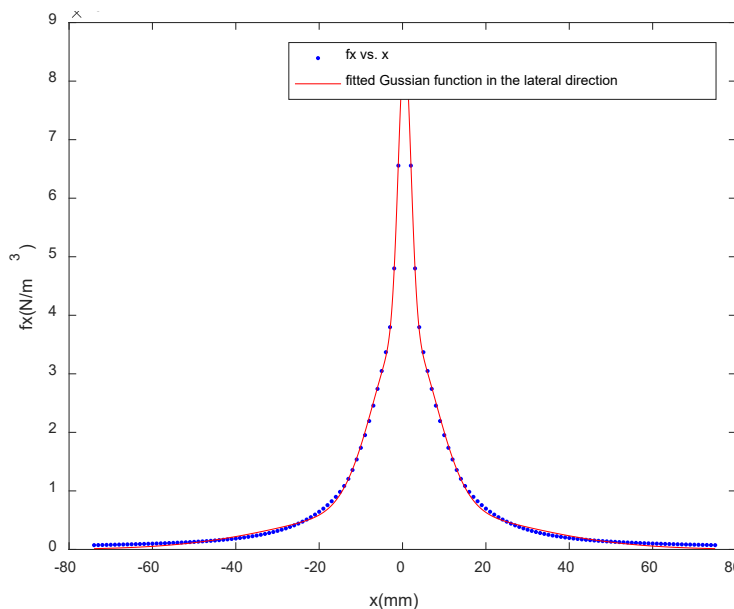
We calculated the mean of the ARF in the axial direction by averaging the amplitude of force in the lateral direction and vice versa. The averaged ARF field in the lateral direction was fitted to a Gaussian function by the curve fitting toolbox in the form of:

$$f(x) = \sum_{i=1}^3 a_i e^{-\frac{(x-b_i)^2}{c_i}}$$

Where a, b and c are constants and

$$f(z) = \sum_{i=1}^4 d_i e^{-\frac{(z-e_i)^2}{f_i}}$$

For the axial direction. Where d, e and f are also constants.



(a)

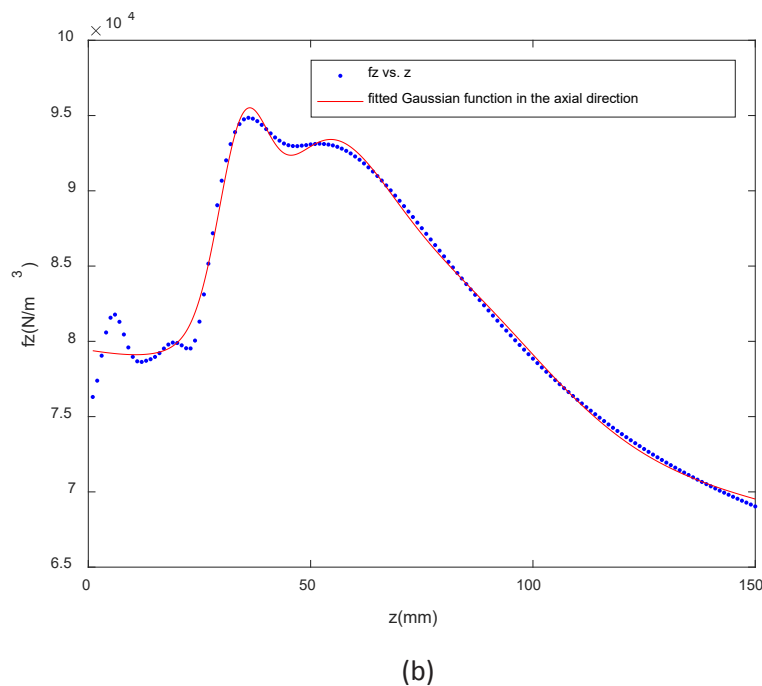


Figure 3. Fitted Gaussian functions in the (a) lateral and (b) axial directions

Different functions such as polynomial, sum of sine, exponential and Gaussian have been used for fitting the force in the lateral and axial directions. Amongst all of them, the Gaussian function with lower terms had the best fitting. Afterwards, we fitted two Gaussian functions in the averaged force in x and z directions. We multiplied these two functions with each other as denoted below:

$$F(x,z)=f(x)*f(z)$$

This function acts as an input body force for FEM and represents the ARF in the x-z plane.

In the part module of ABAQUS, two planes have been created. Upper two dimensional plane is elastic, linear, isotropic and homogeneous while the lower plane is considered as rigid body and was fully-constrained. The upper generated plane has the same dimension with the plane used for pressure calculation (15*15). In the property section, we entered the material properties such as density, Poisson's ratio and elasticity according to the liver tissue. The typical values for tissue characteristics are given in Table 3. Two planes were assembled to each other. In order to obtain a stable solution, time increments must be small enough.

When an AM waveform is used to drive the HIFU transducer, the ARF oscillates at the modulation

frequency. Since we have two sources for exciting the tissue, the closed form of ARF was shifted from the lateral direction to left and right in order to generate two ARF sources.

Table 3. Typical mechanical values which have been entered in the finite element model

Parameter	Value	Unit
Poisson's ratio	0.49	
Density	1000	$\frac{Kg}{m^3}$
Elasticity	10	KPa

Afterwards, these two ARF fields which had been entered as body force in the finite element model, simultaneously oscillated at the modulation frequency. In the amplitude part, we chose the periodic case and entered the Fourier series coefficients of the normalized ARF for each modulation frequency separately. We employed triangular mesh elements in the model. The total number of nodes and elements in the plane is equal to 99088 and 51302, respectively. We used a high viscous material in the outer boundary in the lateral direction which absorbs or reduces the reflected

wave from vertical boundary into the Region Of Interest (ROI) during ARF tissue excitation. The following picture portrays the meshed model. The model was run to complete the process. Therefore,

we can see the results and interference patterns in this part. We used FIELD II for the formation of ultrasound images. The characteristics of the imaging probe are expressed in Table 4.

Table 4. Characteristics of the imaging probe.

Variable name	Value	Unit
Number of elements	128	
Number of active elements	32	
Transducer center frequency	4	MHz
Kerf	0.025	mm
Pitch	0.304	mm
Sampling rate	100	MHz
Focal point	20	mm

The position of the nodes in the first frame of ABAQUS was considered as scatter coordinates in the FIELD II. In the report section of ABAQUS, the displacement of each node in the axial direction in any frame is available. We added this axial displacement to the positions of the nodes in the first frame to reach the new position of scatters. We used 1-dimensional axial cross-correlation

among five sequential images to determine the destructive and constructive points between these two sources.

In a linear elastic and isotropic medium, the shear speed is directly proportional to shear modulus (μ) or Young's modulus (E) and is inversely proportional to density (ρ) and Poisson's ratio (ν)[31]

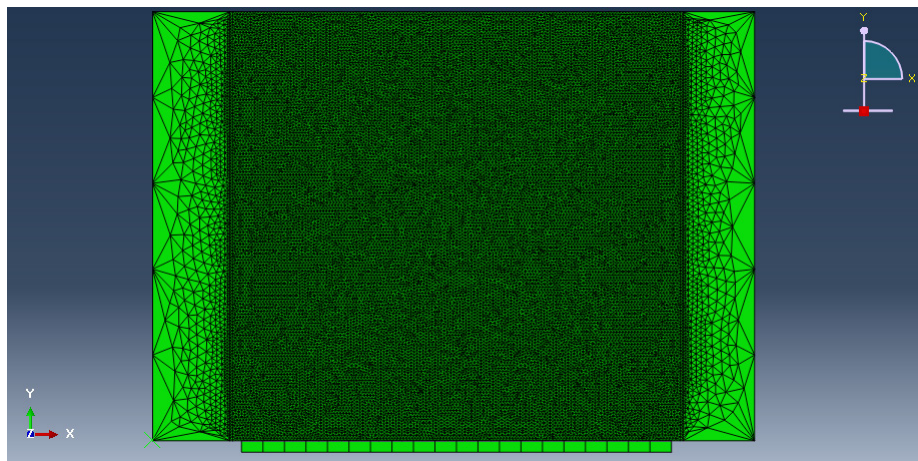


Figure 4.The finite element model using triangular elements

$$C_s = \sqrt{\frac{\mu}{\rho}} = \sqrt{\frac{E}{2(1+\nu)\rho}}$$

Where is the shear wave speed? Since soft tissues are nearly incompressible, the Poisson's ratio is assumed to be 0.5 using the relationship below:

$$E = 3\rho C_s^2$$

The distance between destructive points in these patterns is equal to half the shear wave wavelength. We knew the modulation frequency and by obtaining shear wave wavelength, shear wave speed and consequently Young's modulus were achieved.

3. Results

In this section we investigated the effect of different parameters on shear wave generation and elasticity estimation distinctly.

Figure 5 shows the impact of different excitation frequencies of HIFU transducer from 0.5 to 2 MHz on the elasticity calculation. Modulation frequency, aperture radius and the distance between excitation sources were considered as 100 Hz, 15 mm, and 8 cm respectively.

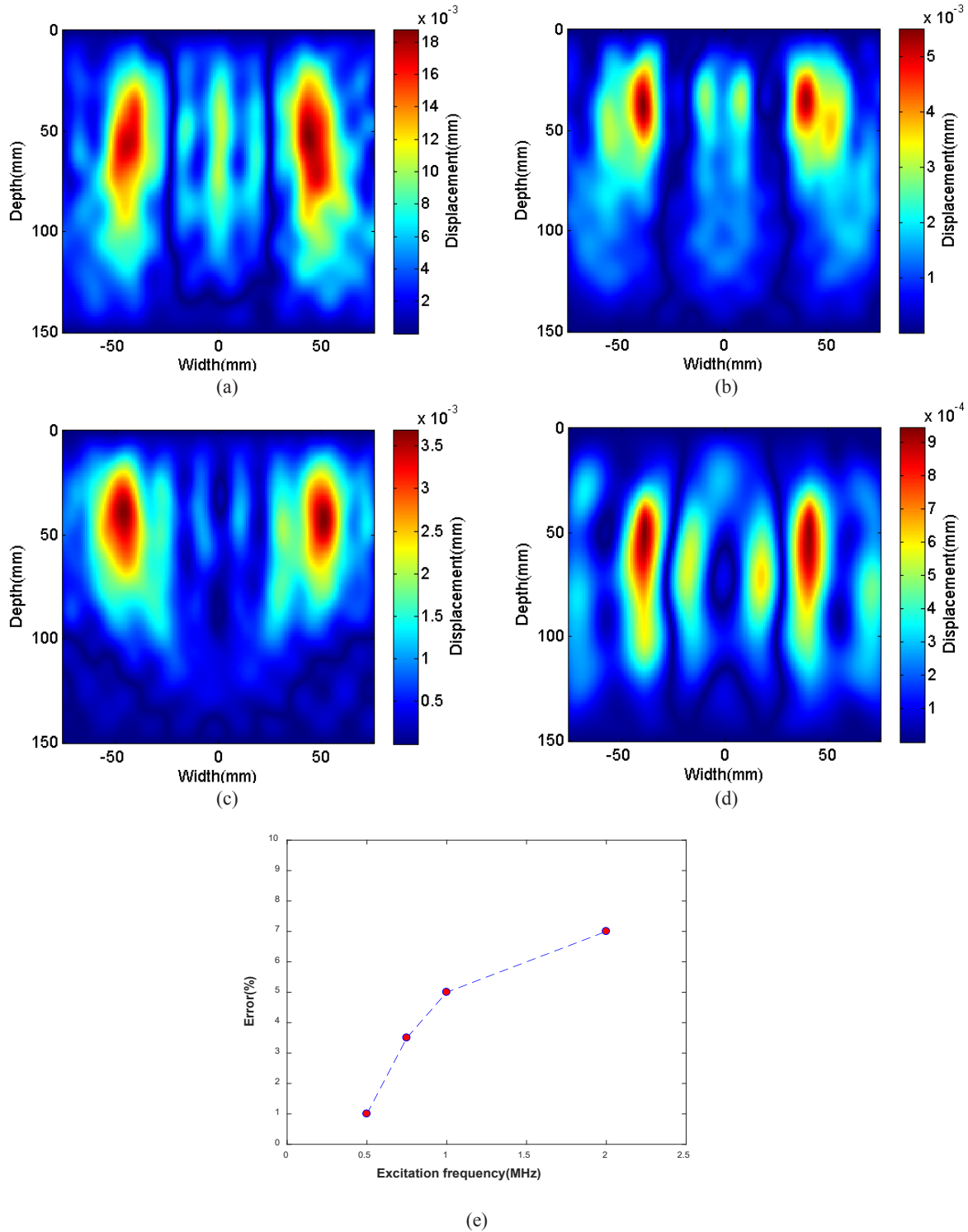


Figure 5. Interference patterns for 500 KHz, 750 KHz, 1 MHz and 2 MHz excitation frequencies are depicted in the (a) to (d) pictures, respectively. (e) Error percentage for different excitation frequencies

The results of varying HIFU transducer’s modulation frequency on the estimation of elasticity are depicted in Figure 6. Modulation frequency was changed to the range of 50 to 150

Hz. Other affecting parameters such as excitation frequency, radius and the distance between sources were considered as 1 MHz, 1.5 cm, 8 cm respectively.

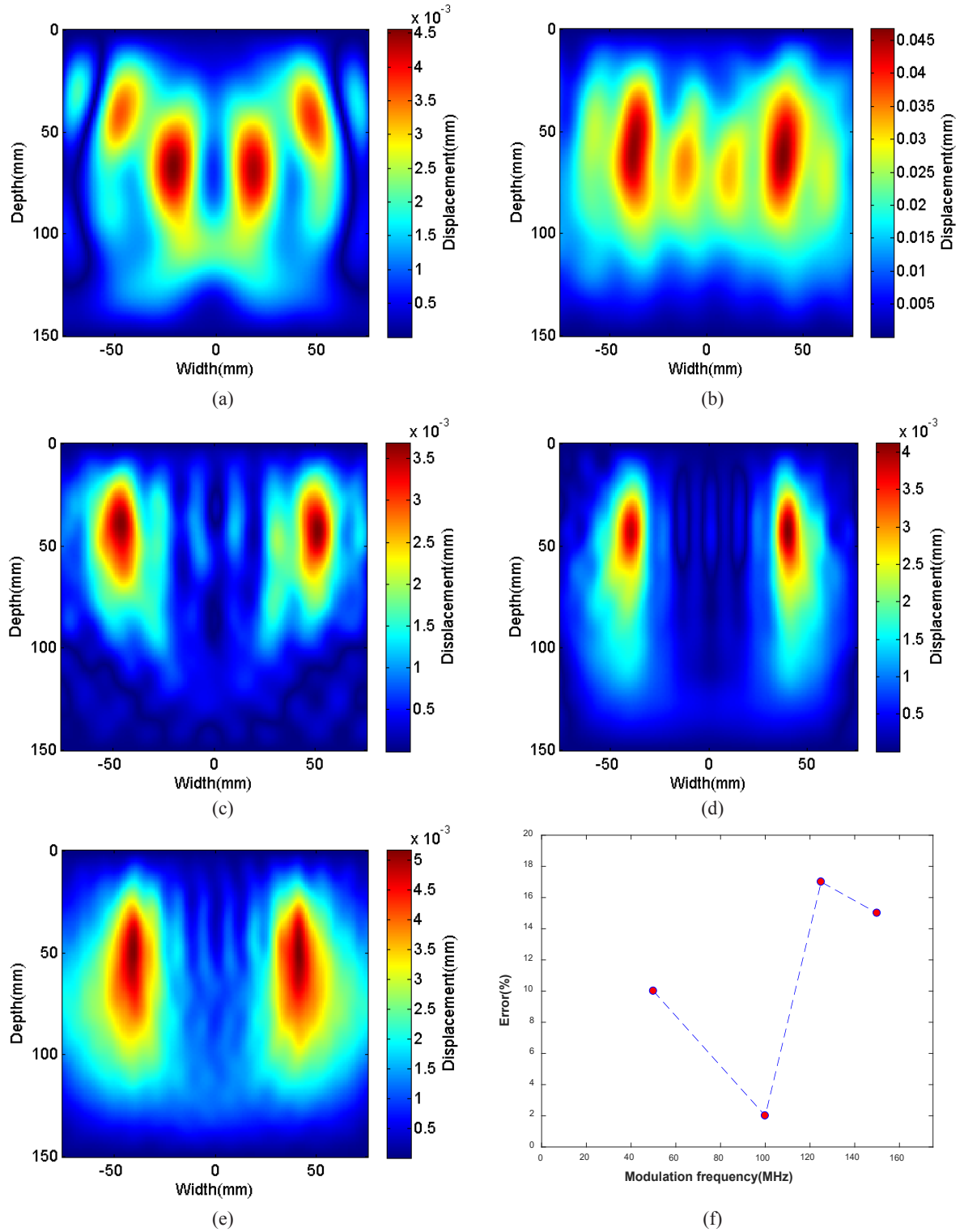


Figure 6. (a) to (e) showing the interference patterns for different modulation frequencies from 50 to 150 Hz with the step size equal to 25 Hz. (f) portrays the percentage error due to varying modulation frequency

Figure 7 shows the results of changing radius of HIFU transducer from 0.75 cm to 2 cm while other parameters such as excitation and modulation

frequency as well as the distance between sources are constant with values 1 MHz, 100 Hz and 8 cm respectively.

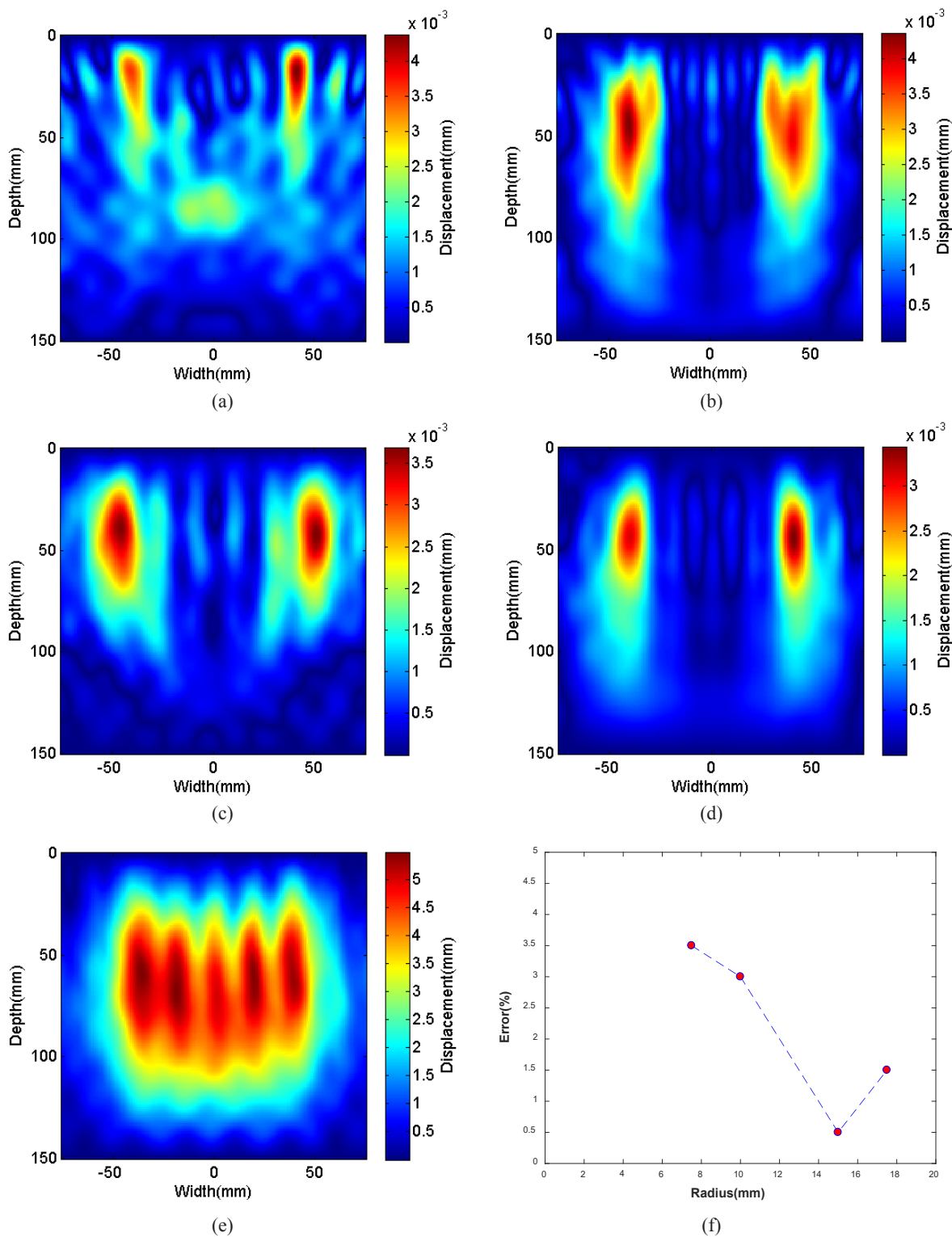


Figure 7. Interference patterns for (a) 7.5 mm (b) 10 mm (c) 15 mm (d) 17.5 mm and (e) 20 mm radius of HIFU. (f) Percentage error for different radius of HIFU

The effect of altering the distances between sources from 6 to 12 cm is shown in Figure 8. Other variables have the same value as the previous test.

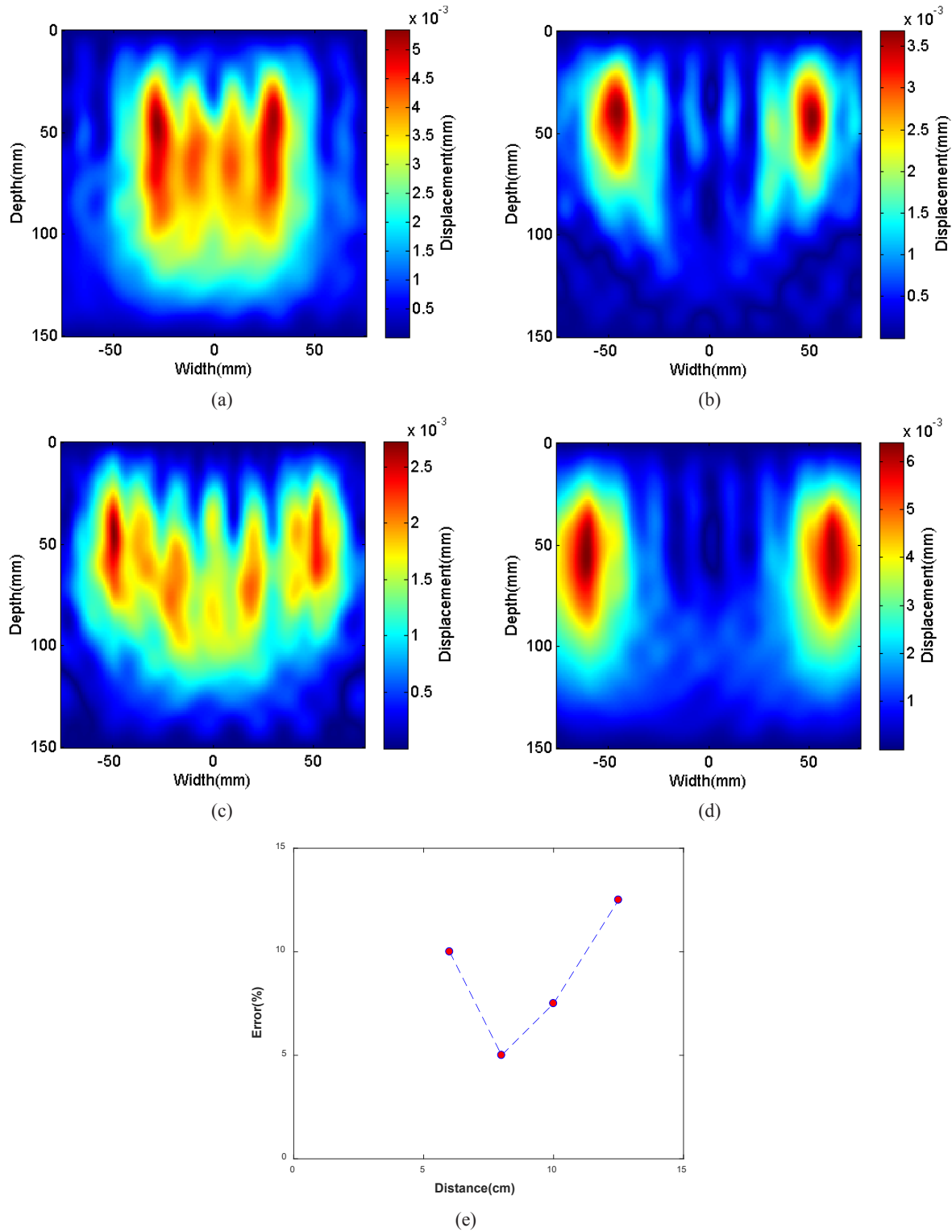


Figure 8. Interference patterns for distances between sources equal to 6,8,10 and 12 cm are displayed in figures (a) to (d); respectively. (e) Error due to the distance between sources

4. Discussion

Shear wave interference pattern elasticity imaging using the acoustic radiation force is a dynamic method that utilizes a harmonically, remotely and oscillatory force in order to displace the tissue. The interference pattern and time-varying radiation force can be generated by radiating the tissue with two separately adjacent AM single frequency HIFU transducer. The induced time-varying force creates the oscillation in tissue at the modulation frequency. This technique is appropriate for a precise estimation of the elasticity variation in tissues due to disease, detection, and monitoring of thermal ablation. In order to reduce the mechanical and cavitation effects, the acoustic pressure was normalized and scaled to the minimum value that can displace the tissue in the range of micrometer in the 1 MHz center frequency. We used corrected DIC MATLAB toolbox which can detect the subsample displacement. For a better estimation of wavelength as well as tissue elasticity, we averaged the distance between destructive points. In order to obtain more accurate results, having one optimization process in choosing different excitation parameters is crucial.

FEM model is able to model a complicated medium and dynamically simulate the tissue response to complex acoustic radiation force.

We chose the excitation frequency of HIFU transducer in the range of 0.5 to 2 MHz. As seen in Figure 5, the percentage error trends upward with increasing center frequency of acoustic sources. One possibility is that with increasing frequency, the attenuation increases and the displacement amplitude decreases. In terms of dB, the attenuation at 1 MHz is twice that at 500 KHz. The focal length is directly proportional to excitation frequency, implying that less excitation frequency results in less attenuation and focal length. For choosing proper frequency, we should compromise between focal depth and attenuation.

In our simulation, the modulation frequency changed from 50 to 150 Hz. As a result of the longer wavelength in lower frequency modulation which cannot be captured by the imaging probe, in addition to the loss of good lateral resolution in high modulation frequencies, the estimated error increased in both cases.

The diameter of transducers varied from 15 to 35 mm. By increasing the radius, the focal length will be longer while the focal spot size decreases. Consequently, the ARF is concentrated in a smaller volume and errors are decreases.

We investigated the effect of the distance between ARF sources from 6 to 12 cm. For small distance sources, the shear waves cannot interfere properly while in larger distances, the wave attenuated. Consequently, for small and large distances, the error increased.

5. Conclusion

In this simulation study, the optimization of affecting variables on shear wave interference patterns utilizing a pair of AM acoustic radiation force was investigated. From the simulations results, we found out that the modulation frequency and the distance between sources are the most affecting parameters. By improving the lateral resolution of the imaging system, the results due to these excitation factors can be improved. Since the aim of our clinical application is the determination of the different degree of liver fibrosis, this method can be used to determine the stages of liver fibrosis with an acceptable error. In future works, shear wave interference patterns in liver tissue by considering the adjacent tissues and the effect of using different push transducers such as phased, curved and linear array transducers can be investigated.

Acknowledgment

This research was supported by Tehran University of Medical Sciences and Health services grant 94-04-30-30919.

References

- 1- H. A. Saleh and A. H. Abu-Rashed, "Liver biopsy remains the gold standard for evaluation of chronic hepatitis and fibrosis," *Journal of Gastrointestinal and Liver Diseases*, vol. 16, no. 4, p. 425, 2007.
- 2- Y. Sumida, A. Nakajima, and Y. Itoh, "Limitations of liver biopsy and non-invasive diagnostic tests for the diagnosis of nonalcoholic fatty liver disease/nonalcoholic steatohepatitis," *World journal of gastroenterology: WJG*, vol. 20, no. 2, p. 475, 2014.
- 3- P. Bedossa, K. Patel, and L. Castera, "Histologic and noninvasive estimates of liver fibrosis," *Clinical liver disease*, vol. 6, no. 1, pp. 5-8, 2015.

- 4- S. K. Venkatesh, M. Yin, and R. L. Ehman, "Magnetic resonance elastography of liver: technique, analysis, and clinical applications," *Journal of magnetic resonance imaging*, vol. 37, no. 3, pp. 544-555, 2013.
- 5- R. Muthupillai, D. Lomas, P. Rossman, J. Greenleaf, A. Manduca, and R. Ehman, "Magnetic resonance elastography by direct visualization of propagating acoustic strain waves," *Science*, vol. 269, no. 5232, pp. 1854-1857, 1995.
- 6- A. Manduca *et al.*, "Magnetic resonance elastography: non-invasive mapping of tissue elasticity," *Medical image analysis*, vol. 5, no. 4, pp. 237-254, 2001.
- 7- K. V. Larin and D. D. Sampson, "Optical coherence elastography—OCT at work in tissue biomechanics," *Biomedical Optics Express*, vol. 8, no. 2, pp. 1172-1202, 2017.
- 8- X. Liu, "Optical coherence elastography," ed: Google Patents, 2018.
- 9- B. F. Kennedy, K. M. Kennedy, A. L. Oldenburg, S. G. Adie, S. A. Boppart, and D. D. Sampson, "Optical coherence elastography," in *Optical Coherence Tomography*: Springer, 2015, pp. 1007-1054.
- 10- S. Wang and K. V. Larin, "Optical coherence elastography for tissue characterization: a review," *Journal of biophotonics*, vol. 8, no. 4, pp. 279-302, 2015.
- 11- A. P. Sarvazyan, O. V. Rudenko, S. D. Swanson, J. B. Fowlkes, and S. Y. Emelianov, "Shear wave elasticity imaging: a new ultrasonic technology of medical diagnostics," *Ultrasound in medicine & biology*, vol. 24, no. 9, pp. 1419-1435, 1998.
- 12- A. Nowicki and K. Dobruch-Sobczak, "Introduction to ultrasound elastography," *Journal of ultrasonography*, vol. 16, no. 65, p. 113, 2016.
- 13- L. Sandrin *et al.*, "Transient elastography: a new noninvasive method for assessment of hepatic fibrosis," *Ultrasound in medicine & biology*, vol. 29, no. 12, pp. 1705-1713, 2003.
- 14- S. Chen *et al.*, "Shearwave dispersion ultrasound vibrometry (SDUV) for measuring tissue elasticity and viscosity," *IEEE transactions on ultrasonics, ferroelectrics, and frequency control*, vol. 56, no. 1, pp. 55-62, 2009.
- 15- H. Xie *et al.*, "Shear wave dispersion ultrasound vibrometry (SDUV) on an ultrasound system: in vivo measurement of liver viscoelasticity in healthy animals," in *Ultrasonics Symposium (IUS), 2010 IEEE*, 2010, pp. 912-915: IEEE.
- 16- C. Maleke and E. E. Konofagou, "Harmonic motion imaging for focused ultrasound (HMIFU): a fully integrated technique for sonication and monitoring of thermal ablation in tissues," *Physics in medicine and biology*, vol. 53, no. 6, p. 1773, 2008.
- 17- E. E. Konofagou and K. Hynynen, "Localized harmonic motion imaging: theory, simulations and experiments," *Ultrasound in medicine & biology*, vol. 29, no. 10, pp. 1405-1413, 2003.
- 18- C. Maleke and E. E. Konofagou, "Harmonic motion imaging for focused ultrasound (HMIFU): a fully integrated technique for sonication and monitoring of thermal ablation in tissues," *Physics in Medicine & Biology*, vol. 53, no. 6, p. 1773, 2008.
- 19- M. Fatemi and J. F. Greenleaf, "Vibro-acoustography: An imaging modality based on ultrasound-stimulated acoustic emission," *Proceedings of the National Academy of Sciences*, vol. 96, no. 12, pp. 6603-6608, 1999.
- 20- M. W Urban, A. Alizad, W. Aquino, J. F Greenleaf, and M. Fatemi, "A review of vibro-acoustography and its applications in medicine," *Current medical imaging reviews*, vol. 7, no. 4, pp. 350-359, 2011.
- 21- G. Ferraioli, P. Parekh, A. B. Levitov, and C. Filice, "Shear wave elastography for evaluation of liver fibrosis," *Journal of Ultrasound in Medicine*, vol. 33, no. 2, pp. 197-203, 2014.
- 22- M. D'Onofrio *et al.*, "Acoustic radiation force impulse of the liver," *World journal of gastroenterology: WJG*, vol. 19, no. 30, p. 4841, 2013.
- 23- K. Nightingale, M. S. Soo, R. Nightingale, and G. Trahey, "Acoustic radiation force impulse imaging: in vivo demonstration of clinical feasibility," *Ultrasound in medicine & biology*, vol. 28, no. 2, pp. 227-235, 2002.
- 24- J. Bercoff, M. Tanter, and M. Fink, "Supersonic shear imaging: a new technique for soft tissue elasticity mapping," *IEEE transactions on ultrasonics, ferroelectrics, and frequency control*, vol. 51, no. 4, pp. 396-409, 2004.
- 25- W. J. Choi, J. S. Park, H. R. Koo, S.-Y. Kim, M. S. Chung, and K. Tae, "Ultrasound elastography using carotid artery pulsation in the differential diagnosis of sonographically indeterminate thyroid nodules," *American Journal of Roentgenology*, vol. 204, no. 2, pp. 396-401, 2015.
- 26- Z. Wu, L. S. Taylor, D. J. Rubens, and K. J. Parker, "Sonoelastographic imaging of interference patterns for estimation of the shear velocity of homogeneous biomaterials," *Physics in medicine and biology*, vol. 49, no. 6, p. 911, 2004.

- 27- J. R. Doherty, G. E. Trahey, K. R. Nightingale, and M. L. Palmeri, "Acoustic radiation force elasticity imaging in diagnostic ultrasound," *IEEE transactions on ultrasonics, ferroelectrics, and frequency control*, vol. 60, no. 4, pp. 685-701, 2013.
- 28- Z. Hah, C. Hazard, Y. T. Cho, D. Rubens, and K. Parker, "Crawling waves from radiation force excitation," *Ultrasonic imaging*, vol. 32, no. 3, pp. 177-189, 2010.
- 29- K. Hoyt, Z. Hah, C. Hazard, and K. J. Parker, "On the use of dual acoustic radiation forces to induce shear wave propagation and interference pattern formation," in *Ultrasonics Symposium (IUS), 2012 IEEE International*, 2012, pp. 2583-2586: IEEE.
- 30- M. L. Palmeri, S. A. McAleavey, G. E. Trahey, and K. R. Nightingale, "Ultrasonic tracking of acoustic radiation force-induced displacements in homogeneous media," *IEEE transactions on ultrasonics, ferroelectrics, and frequency control*, vol. 53, no. 7, pp. 1300-1313, 2006.
- 31- M. L. Palmeri, A. C. Sharma, R. R. Bouchard, R. W. Nightingale, and K. R. Nightingale, "A finite-element method model of soft tissue response to impulsive acoustic radiation force," *IEEE transactions on ultrasonics, ferroelectrics, and frequency control*, vol. 52, no. 10, pp. 1699-1712, 2005.